PROTON MR TWO - COMPONENT CHEMICAL SHIFT IMAGING OF FLUIDS IN POROUS MEDIA

C.T. Chang and C.M. Edwards
Engineering Imaging Laboratory
Texas A&M University
College Station, TX 77843-3116

ABSTRACT

An NMR chemical shift imaging modality is presented for quantitative determination of the spatial distribution of water and oil saturation in porous samples. It is applicable to those samples for which the two resonance lines overlap severely, and for which significant signal decay occurs during the chemical shift evolution period. We have used this method to demonstrate the separation of water and oil images in sand packs and core samples.

INTRODUCTION

Magnetic resonance imaging (MRI) has the potential to provide a means to determine the spatial distribution of fluid saturations within opaque porous media, with obvious applications in rock physics, fluid/rock interfacial processes, and porous media fluid dynamics, especially liquid - liquid displacement mechanics. In order to study the multiphase flow, where several fluid phases may be present within the pore space, it is necessary to distinguish between fluids of different chemical compositions.

During the last few years, several approaches for achieving this result have been investigated. Hall et al.[1] performed a study in which they obtained resolved images of water and oil in a sandstone based on the difference in relaxation times. However, it is necessary that the protons in different phases have different relaxation times. Relaxation times of fluids in porous media are dominated by fluid/surface interactions and pore geometry[2], resulting in a wide distribution of relaxation times as well as a decrease in the difference of relaxation times between water and oil. Consequently, the available contrast for fluid identification based on relaxation times is considerably reduced. A number of other workers have reported NMR images of water and oil distributions in porous samples utilizing the chemical shift interaction. The various methods for chemical shift imaging can be classified into two major categories. The first category consists of methods that selectively excite or saturate water (or oil) protons before a conventional imaging pulse sequence is applied. Edelstein, et al.[3] have demonstrated the use of selective excitation to observe oil and water in saturated dolomite cores. The selective saturation method has been used by Dechter, et al.[4] to obtain specific images for Bakers dolomite and Bentheim sandstone core. The spectrally selective pulses again yield images of only one fluid phase at a time. The second category involves methods of spectroscopic chemical - shift imaging, in which a chemical - shift dimension is added to each voxel. Conventional chemical - shift imaging uses two spatial orthogonal phase - encoding magnetic field gradients and collects free induction decay signals in the absence of magnetic field gradients.[5] Hall et al.[6] used this technique to observe dodecane and water in Berea sandstone samples. The full three - dimensional chemical - shift imaging methods are rarely used because of long experiment times, unless relatively coarse spatial resolution is acceptable. If high spectral resolution is not desired, the data acquisition efficiency can be enhanced significantly by frequency encoding one of the space dimensions and phase encoding the chemical shift. In a spin - echo sequence this is usually done by changing the amplitude of the magnetic field gradient pulse[7] or by varying the time of the 180° pulse while keeping the time between excitation and acquisition constant.[8] By making one of these changes a

time delay is inserted between the Hahn spin - echo and gradient echo allowing the magnetization vectors to evolve out of phase with each other by an amount dependent on the spectral frequency differences. If this period is incremented in regular steps, the spectral frequency will be encoded as a phase change, yielding the desired spectrum upon Fourier transformation. Majors, et al.[9] reported the use of the echo - time - encoded spectroscopic imaging technique to study the displacement of oil by water - flooding in a dolomite core sample.

It can be seen that the application of all the above techniques is limited to those samples for which the NMR line broadening is moderate and spectral resolution is still observable. Horsfield, et al.[10] presented an estimation method based on the phase shift technique to observe water and dodecane in a Hopeman sandstone. This method provides the ability to distinguish two chemically - shifted components even when the spectral lines cannot be resolved. Well - characterized spectra and a large amount of computing power are required to be successful using this technique. In addition the quantification of the intensity of the NMR signal is problematical. We present here an improvement upon Horsfield's technique for chemical shift imaging which provides the capability to rapidly and easily quantify the oil and water NMR signals in porous media where their resonance lines are not baseline separated.

THEORY AND METHODS

The imaging sequence used was a modified spin - warp spin - echo sequence (Fig. 1) into which a variable chemical - shift evolution time τ is introduced. The gradient echo always occurs at a time t when

$$\int_0^t G(\tau')\, d\tau' = 0. \qquad (1)$$

It is at this time that the frequency encoded position information is in phase. All other frequency encoded information such as chemical shift and inhomogeneous line broadening are in phase at the Hahn spin echo time. Deliberately allowing the Hahn echo and the gradient echo to occur at different times is the method for introducing the chemical - shift evolution time τ. Using the knowledge of the chemical shift between oil and water, a phase shift of the respective signals can be achieved by suitable adjustment of Hahn spin - echo time relative to gradient echo time . Since a chemical - shift dimension is generated only to resolve the different fluids, high spectral resolution is not required. As demonstrated by Dixon,[11] two steps of evolution period may be adequate to resolve two fluid phases.

The Dixon method, however, suffers from two drawbacks with respect to quantitative accuracy when applied to fluids in porous media. First, when chemical - shift evolution takes place, factors other than chemical shift can cause additional phase shifts. These factors include inhomogeneity of the static magnetic field, magnetic susceptibility variations and nonuniform phase delays caused by instrumentation factors such as induced eddy currents of time dependent magnetic fields. Second, during the period of chemical shift evolution the signal from each pixel will decay with time constant T_2^*, where T_2^* is associated with the linewidth for the pixel in question. Therefore, to quantitatively resolve water and oil signals it is necessary to (a) remove the contribution of phase errors due to nonchemical shift mechanisms, and (b) take into consideration the signal decay.

Let (x,y) be coordinates in the laboratory frame of reference, which is perpendicular to the slice selection direction z. In the two dimensional spin warp Fourier transform MRI technique, the free induction decay signal can be expressed as[8]

$$S(t,G_y) = \int d\omega \int dx \int dy\ \rho(x,y,\omega)$$
$$\exp\{i[(\omega + \Delta)(t+\tau) + \gamma G_x x t + \gamma G_y y t_y + \alpha]\}\ , \tag{2}$$

where G_x and G_y are the gradients in x and y directions, respectively; γ is the gyromagnetic ratio; $\Delta(x,y)$ is the frequency offset due to the magnetic field inhomogeneity; t_y is the time for which the phase encoding gradient G_y is switched on; and $\alpha(x,y)$ is the nonuniform phase delays caused by instrumentation factors. The expression $\rho(x,y,\omega)$ is the spin density including the relaxation effects, where ω is written explicitly to specify that the image signal is subject to the linewidth and chemical shift effects. The signal is collected as a function of time t after the read gradient G_x is on. One may show[12] that Eq. 2 is the result of neglecting the fact that the protons with different chemical shift are excited at slightly different positions along the z-axis corresponding to their resonance frequencies. Therefore, Eq. 2 may be used within experimental error when a sufficiently large z-gradient is applied during the excitation period. This condition for the slice definition is assumed throughout this paper.

An NMR image is obtained by Fourier transforming Eq. 2 with respect to G_y and t. One can see that the conjugate variable of G_y is $\gamma y t_y$, which is readily transformed to y since γ and t_y are known quantities. However, the Fourier transform variable of t is $(\omega + \Delta + \gamma G_x x)$; thus the effects of linewidth, chemical shift and field inhomogeneity are to spread out the signal in the x-direction in the image. For a sufficiently strong gradient G_x, the misregistration in the readout direction can be small. In this work this offset is less than 1 pixel. Under this condition the image intensity for each pixel is of the form

$$S(x,y) = \left\{\int \rho(x,y,\omega)\, e^{i\omega\tau}\, d\omega\right\} \cdot \exp\{i(\Delta \cdot \tau + \alpha)\}\ . \tag{3}$$

When a sample consists of two chemical components with chemical shift δ_k and lineshape function $f_k(\omega)$, $\rho(x,y,\omega)$ can be partitioned into two parts, $\sum_{k=1,2} \rho_k(x,y)\, f_k(\omega - \delta_k)$, and Eq. 3 can be rewritten as follows:

$$S(x,y) = \left\{\sum_{k=1,2}\left[\int f_k(\omega')\, e^{i\omega'\tau}\, d\omega'\right] \rho_k(x,y)\, e^{i\delta_k\tau}\right\} \cdot \exp\{i(\Delta \cdot \tau + \alpha)\}\ , \tag{4}$$

where $\omega' = \omega - \delta_k$. The integration

$$g_k(\tau) = \int f_k(\omega') e^{i\omega'\tau} d\omega' \quad , \tag{5}$$

which is the Fourier transform of the lineshape function, represents a decay factor of the signal during the period τ. For a Lorentzian lineshape, the decay factor is simply $\exp(-|\tau| / T_2^*)$.

If the transmitter reference frequency is placed at the nominal precessional frequency of water protons, Eq. 4 becomes

$$S(x,y) = \{g_w(\tau)\rho_w + e^{i\delta\tau} g_o(\tau) \rho_o\} \cdot \exp\{i(\Delta \cdot \tau + \alpha)\} , \tag{6}$$

where $g_{w,o}$ and $\rho_{w,o}$ are the signal decay factor and spin density, respectively, for water/oil; and δ is the chemical shift of oil signal relative to water signal. The transmitter is not required to be at the water proton frequency. If some offset exist it is simply added to Δ.

The in - phase ($\delta\tau = 0$) and opposed - phase ($\delta\tau = \pi$) images can be used to determine the position dependent phase factor $\Delta \cdot \tau$. To do this, the phase errors α caused by instrumentation factors are first removed from the opposed - phase image by rotating the intensity vector of each pixel by an angle $-\alpha$, where α is the phase angle of the corresponding pixel in the in - phase image. A phase slope method[13] is then used to remove any abrupt 180° transitions in the phase of the opposed - phase image at water/oil interfaces. This leaves only the smooth phase shifts $\Delta \cdot \tau$. Phase unwrapping is required in the cases when $\Delta \cdot \tau$ is of such magnitude that phase wraparound problem must be confronted, which often occur for images of large cross - sectional area or for samples with large magnetic susceptibilities.

Instead of using in - and opposed - phase images to obtain segregated water and oil images, two more images are acquired by shifting the Hahn spin - echo before and after the field gradient echo, giving symmetric 90° phase shift of the oil magnetization vector with respect to the water vector. By so doing, the problem of different signal decay factors can be minimized since the chemical - shift evolution time is the same in both image data sets. The images are phase corrected with phase map $\Delta \cdot \tau$ /2, where $\Delta \cdot \tau$ is obtained from the opposed-phase image. In accordance with Eq. 6, vector diagrams of the magnetic moments with $\delta\tau = \pm 90°$ in the rotating frame are drawn, as shown in Fig. 2. The phase shifts due to field inhomogeneities have been corrected and the phase delay α is not shown for clarity. At each voxel the signal, S(x,y), will have decayed because of the T2* effects. This is represented by spreading of vectors representing oil and water magnetization. In the figure these line widths of the oil and water resonances are equal. Because the net magnetization for the oil/water components is the vector sum of the oil/water isochromats, net magnetization will be ±90° out of phase regardless of the oil/water linewidths

There are two points to be noted in Fig. 2. First, in general cases the water and oil resonance lines can be overlapping. Second, the signal decay factor is determined by the lineshape and can be different for the two fluids. When the lineshapes for the two fluids are different, then quantification is difficult unless the linewidths have been determined independently. For fluids in porous media the linewidth is dominated by microscopic field gradients caused by the static susceptibility difference between the fluids and the rock matrix combined with the random geometry of the pore space.[14] If the aqueous phase does not have too many dissolved

paramagnetic impurities then the static susceptibility of the aqueous phase and the oil phase should not be very different and the linewidths of the two phases would therefore be approximately equal. But even under the conditions where the linewidths are significantly different, it is apparent from the diagrams that the vector sum and difference of these two image data sets yield the completely separated component vectors. The final separated images can then be formed in magnitude to eliminate the phase factor α.

RESULTS AND DISCUSSION

All measurements were performed on a General Electric 2T CSI system operating at 85.56 MHz, with an Oxford instrument superconducting magnet of 31 cm diameter horizontal bore, supported by a Nicolet 1280 computer together with a Nicolet 293F pulse programmer. Magnetic field gradients were provided by a shielded Accustar gradients set with 200 μs settling time. An 11 cm birdcage RF probe was used for both radiofrequency transmission and reception of the NMR signal.

The pulse sequence used is shown in figure 1. It is an ordinary 2-D spin warp sequence except the Hahn - echo time is allowed to vary while the gradient - echo time is kept fixed. This is accomplished by changing the timing of the 180° inversion pulse. Precise control over the oil/water phase shift is possible using this method. The only limitation is that t must be much less than T2 in order to neglect T2 effects in the analysis of the data.

The first porous sample used in this study was a composite sample which was made from a cylindrical vial (1.0 cm i.d. and 3.5 cm length) of Ottawa sand (50 - 70 mesh). Water and machine oil were absorbed separately into the two halves of the sample. By examining the NMR spectrum, it was observed that the proton resonances of water and oil are separated by 3.5 ppm and the linewidth at half-maximum for each of the resonances was estimated to be approximately 2.4 ppm. The longitudinal relaxation times T_1 for the water and oil in the sample were measured to be 133 and 116 ms, respectively. The transverse relaxation times T_2 were measured using the Hahn sequence and were found to be 20 and 28 ms, respectively. One - dimensional projection images were taken along the cylindrical axis of the sample which is in the vertical direction. The time between the 90° pulse and the center of the gradient echo is 4 ms. In order to achieve a 180° phase shift between the oil and water resonances, an evolution time of 1.6 ms was used. Two hundred fifty -six complex points were collected during the echo, giving a resolution of 0.17 mm. Figure 3 is an in phase image upon magnitude calculation. The water occupies the lower part of the sample and the interface between water and oil is in the vicinity of the 120th pixel. Figure 4 compares the present method with the Dixon method. Fig. 4 (a) and (b) were calculated by summing and subtracting the in - phase and opposed - phase image vectors, respectively. It is noted that some oil intensities remain in the water image and likewise, some water intensities are seen in the oil image. As mentioned earlier, the artifact is due to static field inhomogeneity errors as well as the difference in the signal decay factors between in - and opposed - phase images. Fig. 5 is a phase map of inhomogeneity and magnetic susceptibility as calculated from the opposed - phase image. It is a function which varies smoothly over the sample with discontinuities at the boundary between the sample and the surrounding area. The effect of the magnetic field inhomogeneity on the pore - size scale can be averaged over each pixel because the pixel size is generally larger than the pore size. Fig. 4 (c) and (d) are the true water and oil images, respectively, obtained using our method, which show a clear separation of the two fluids.

Next, we demonstrated the ability of this method to resolve two chemically distinct fluids coexisting as immiscible phases intimately mixed in the same pore space. The rock samples used in this experiment were Bentheim sandstone, the cores being 2.54 cm in diameter and 4.7 cm long and having a porosity of 23%. Three identical cores were prepared: the first one was 100% saturated with 5% sodium chloride solution (specific gravity 1.034); the second one was 100%

saturated with Soltrol 130 (specific gravity 0.754); whereas the third one was flushed through with approximately 31 pore-volumes of Soltrol 130 after the 100% brine saturation. Fig. 6 shows a spectrum from the third sample. The linewidth for each resonance was measured from the single - fluid saturated samples to be 3.2 ppm for water and 3.3 ppm for oil, satisfying the requirement for quantification of the fluid phase. The relaxation times T_1 and T_2 are 628 ms (716 ms) and 16.6 ms (19.1 ms) for the water (oil) saturation, respectively. Transverse slice images with three samples bundled together were taken. The slice - select gradient was 1.94 G/cm, which gave a slice thickness of 5 mm. One hundred twenty - eight complex points were sampled in the presence of 3 G/cm readout gradient, which, combined with 128 increments of the phase - encoding gradient gave an in - plane resolution of 0.5 mm. The time between the excitation pulse and acquisition was 3.6 ms. A phase map associated with the magnetic field inhomogeneity was calculated from the phase difference between the opposed - and in - phase image data sets, and which was subsequently used in the correction of the ± 90° phase - shifted image data. Fig. 7 shows the separated water and oil images obtained by using our method. The water and oil signal intensities were then calculated from the NMR images by summation of the pixel intensities over the regions of the images in which the cores sit. The results are shown in Table 1, together with the values calculated from the ordinary image. The remaining intensity of the 100% water (oil) saturated sample in the oil (water) image is less than 4%. If we treat the cores which contain single - fluid saturation as standard references, the combined signal intensity from water and oil in the mixed saturated core is found to be in excellent agreement with the value obtained from the ordinary image.

Table 1. Average Signal Intensity in Bentheim Sandstone

Sample	Chemical - Shift Image		Ordinary Image
	Water Image	Oil Image	
Background	599	586	423
Water saturated	25,538	1,005 (3.9%)	15,239
Oil saturated	1,063 (3.8%)	28,247	17,792
Water & Oil Saturated	13,722	11,728	15,606

We have also used this method to study the oil - flooding of the water saturated rock sample. A cylindrical sample of carbonate (2.5 cm diameter, 5.5 cm length) was oven dried at 70°C for 24 hours and then vacuum saturated with 2% sodium chloride solution. At this stage, the water saturation was 100% and the porosity of the sample was found to be approximately 20%. The core was then inserted into a plastic core holder with a Hassler sleeve and an external pressure of 120 psi was applied on the Hassler sleeve and so maintained during the entire experiment. The core was injected with machine oil at a rate of 0.1 ml/min using an HPLC pump. The NMR spectrum linewidth is 236 Hz at 2 Tesla, and T_1 and T_2 are respectively 123 and 7.6 ms. Two hundred fifty - six phase - encoding steps and 256 complex points were sampled in the presence of a 5G/cm gradient in the flow direction (Z - direction), which allowed the time between 90° pulse and acquisition to be reduced to 4.3 ms and gave an in - plane resolution of 0.27 mm. Again the slice thickness was 5 mm. With eight averages for each image data the experiment time was 17 minutes. The flow was interrupted during the performance of the experiments. Fig. 8 shows a time - lapse series of the spatially resolved water and oil saturations of the water displacement by oil in the core. The horizontal direction is Z which corresponds with the readout gradient, the cylindrical axis of the core, the direction of the applied magnetic field, and the direction of the flow (from right to left), whereas the vertical direction is Y. The displacement of water by oil is seen to proceed with well - behaved phase boundaries. The field inhomogeneity correction algorithm was successfully applied to each image data, though the opposed - phase image has reduced amplitude

in those regions where the water and oil coexist, resulting in a relatively noisy phase map. In case the signal intensity for the opposed - phase image is too weak to produce a useful phase map, a phase correction can be performed using the one generated from the data set where the water saturation was 100%. [10]

CONCLUSION

An efficient method of chemical shift imaging has been presented. The method involves only a simple modification of the technique described by Horsfield together with a phase correction algorithm. It can easily be extended to a multislice experiment by using slice-selective excitation pulses in the usual way. One of the main advantages of this method is its availability of quantitatively mapping water and oil distribution in porous rocks even when the resonance lines overlap. Another advantage is time efficiency as compared to a full three-dimensional chemical shift imaging experiment. One disadvantage is that an opposed phase image with poor signal-to-noise ratio may result from regions where the signal intensities from the water and oil are approximately the same, making the phase correction difficult. We have successfully demonstrated the quantitative separation of water and oil images in sand packs and some rock samples. The chemical shift imaging technique described here appears to improve the possibility of quantitative analysis of the spatial distribution of the fluid phases in core samples.

REFERENCES

1. L.D. Hall and V. Rajanayagam, Thin - Slice, Chemical - Shift Imaging of Oil and Water in Sandstone Rock at 80 MHz, Journal of Magnetic Resonance **74**, 139 (1987)

2. F. D'Oraxio, J.C. Tarczon, W.P.Halparin, K. Eguchi, and T. Mizusaki, Application of Nuclear Magnetic Resonance Pore Structure Analysis to Porous Silica Glass, J. Appl. Phys. **65**, 743 (1989)

3. W.A. Edelstein, H.J. Vinegar, P.N. Tutunjan, P.B. Roemer and O.M. Mueller, NMR Imaging for Core Analysis: SPE 18272, 63rd Annual Technical Conference and Exhibition, October 1988

4. J.J. Dechter, R.A. Komoroski and S. Ramaprasad, NMR Chemical Shift Selective Imaging of Individual Fluids in Sandstone and Dolomite Cores, SCA Conference paper number 8903, 1989

5. L.D. Hall and S. Sukumar, Three - dimensional Fourier Transform NMR Imaging, J. Magn. Reson., **56**, 314 (1984)

6. L.D. Hall, V. Rajanayagan, and C. Hall, Chemical - Shift Imaging of Water and n-Dodecane in Sedimentary Rocks, J. Magn. Reson., **68**, 185 (1986)

7. J.J. Ford, Gradient - Amplitude Phase - Encoded Spectral Imaging. A Novel Approach to Spin - Echo Chemical - Shift Imaging, J. Magn. Reson., **87**, 346 (1990)

8. C.C. Lodes, J.P. Felmlee, R.L. Ehman, C.M. Sehgal, J.F. Greenleaf, G.H. Glover, and J.E. Gray, Proton MR Chemical Shift Imaging Using Double and Triple Phase Contrast Acquisition Methods, Journal of Computer Assisted Tomography **13(5)**, 855 (1989)

9. P.D. Majors, J.L. Smith, F.S. Kovarik, and E. Fukushima, NMR Spectroscopic Imaging of Oil Displacement in Dolomite, J. Magn. Reson, **89**, 470 (1990)

10. M. Horsfield, C. Hall, and L.D. Hall, Two - Species Chemical - Shift Imaging Using Prior Knowledge and Estimation Theory. Application to Rock Cores, J. Magn. Reson., **87**, 319 (1990)

11. W.T. Dixon, Simple Proton Spectroscopic Imaging, Radiology **153**, 189 (1984)

12. A. Volk, B. Tiffon, J. Mispelter, and J. M. Lhoste, Chemical Shift Specific Slice Selection, A New Method for Chemical Shift Imaging at High Magnetic Field, J. Magn. Reson., **71**, 168 (1987)

13. J.A. Borrello, T.L. Chenevert, C.R. Mayer, A.M. Aisen, and G.M. Glazer, Chemical Shift - based True Water and Fat Images: Regional Phase Correction of Modified Spin - Echo MR Images, Radiology, **164**,531 (1987)

14. J.A. Glael and K.H. Lee, On the interpretation of water nuclear magnetic resonance relaxation times in heterogeneous systems, J. Am. Chem. Soci., **96(4)**, 970 (1974)

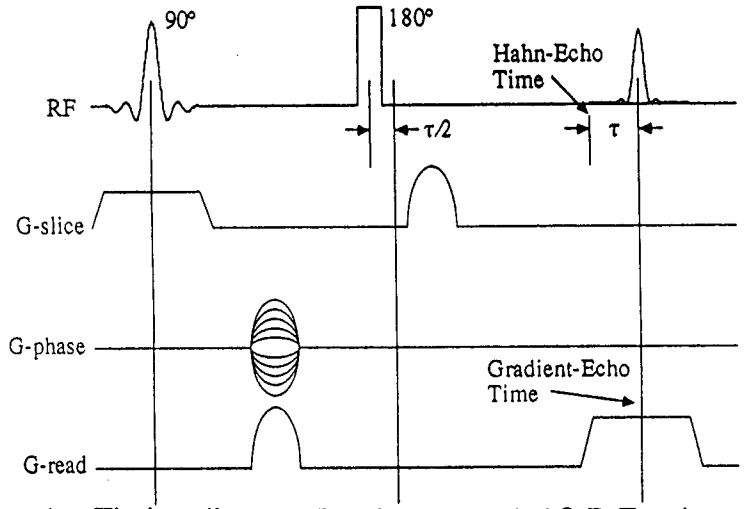

Figure 1. Timing diagram for phase-encoded 2-D Fourier transform chemical-shift imaging pulse sequence.

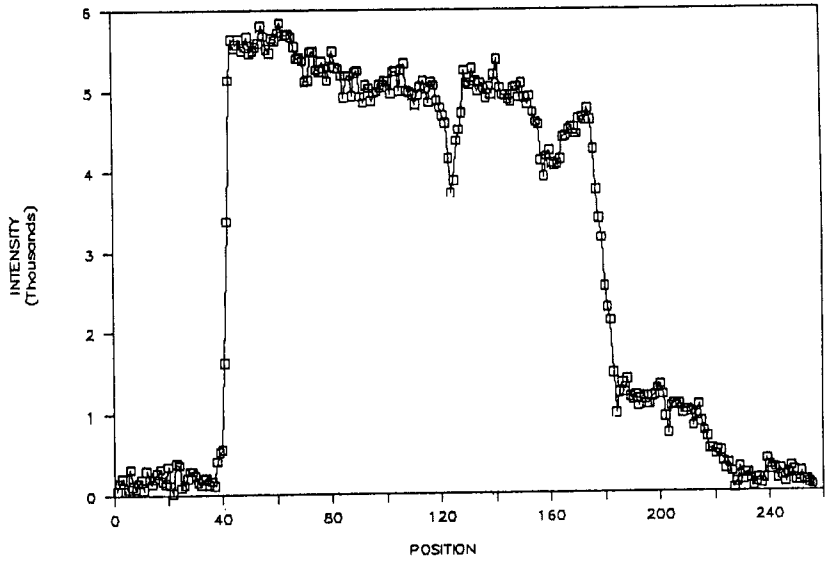

Figure 3. Conventional 1-D profile image of the composite sand pack sample. The magnitude calculation was carried out to obtain the image of water and oil.

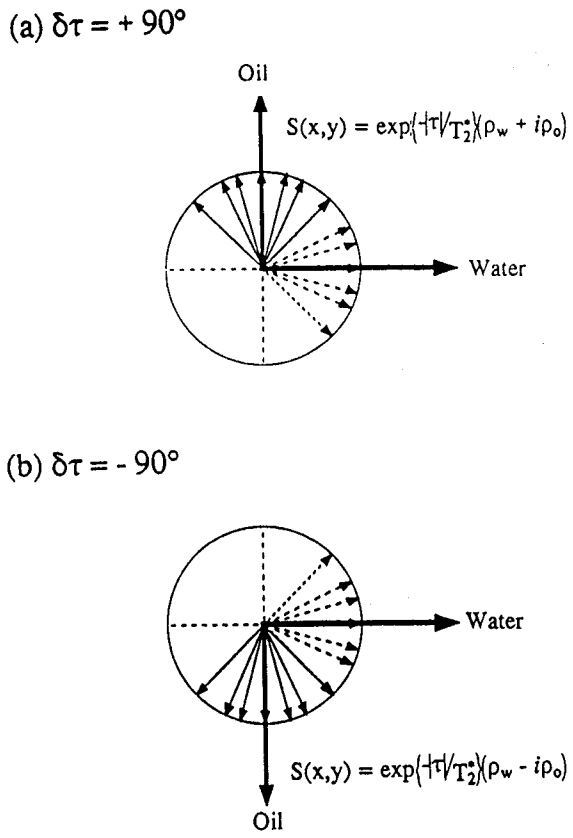

Figure 2. Proton magnetic moments for a pixel containing both water and oil, representing the signals obtained at times when (a) $\delta\tau = +90°$ and (b) $\delta\tau = -90°$. They are drawn in a frame rotating at the water proton frequency. The dashed vectors represent water magnetization and the solid vectors represent oil magnetization.

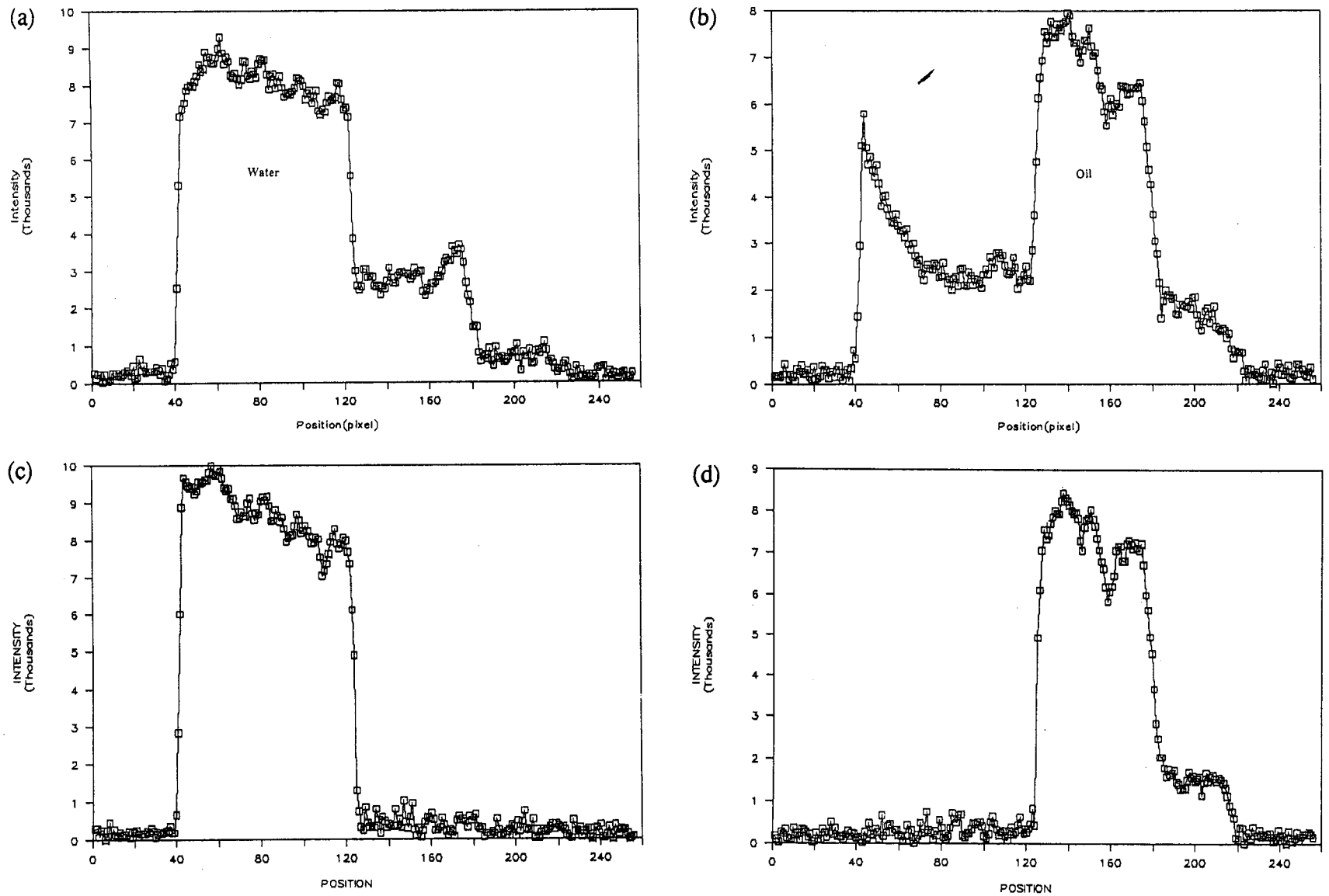

Figure 4. Chemical-shift 1-D profile images of the sand pack sample containing water and machine oil. (a) and (b) are the water and oil images, respectively, obtained using magnitude-of-sum and difference techniques (Dixon's technique). (c) water image, and (d) oil images obtained using method described in the text.

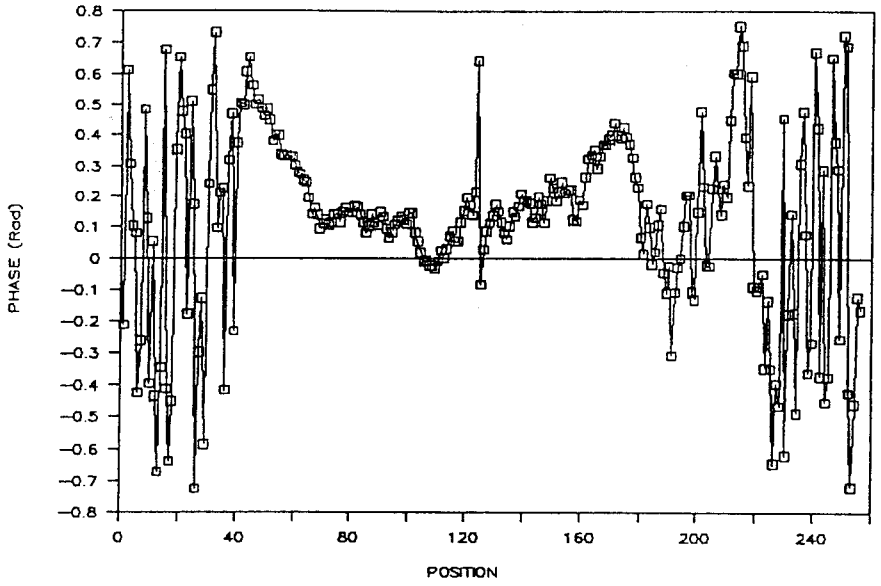

Figure 5. One-dimensional phase map of the sand pack sample showing the nonchemical-shift phase effects.

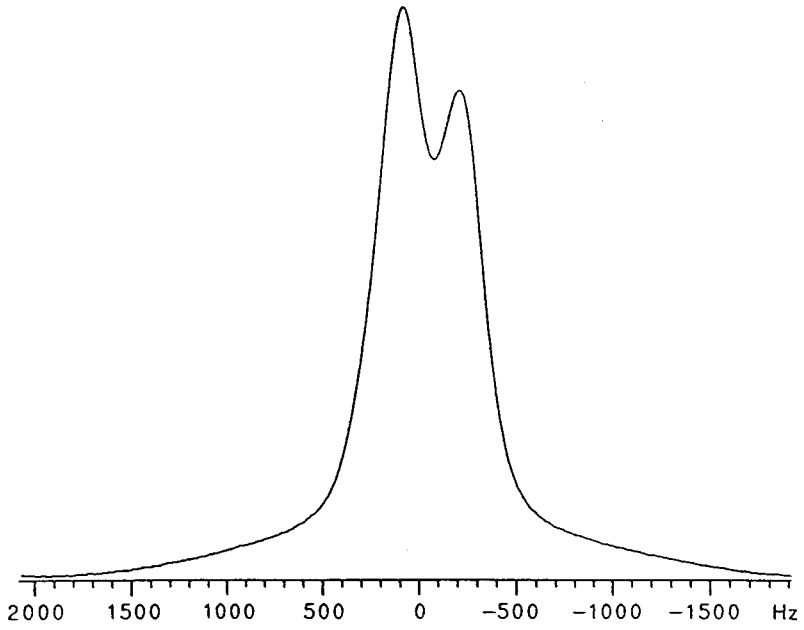

Figure 6. NMR spectrum taken from the whole Bentheim sandstone sample with mixed oil and NaCl solution saturations.

(a)

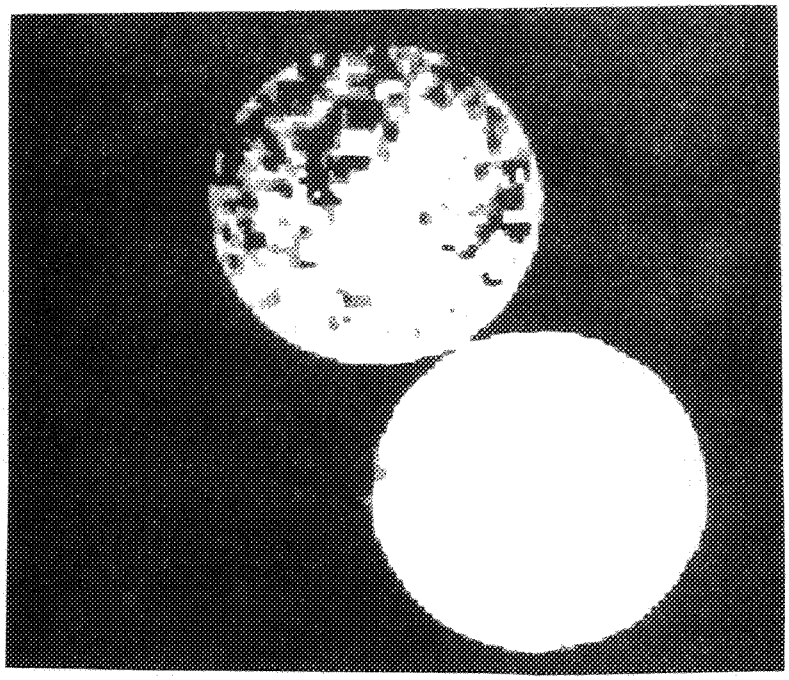

(b)

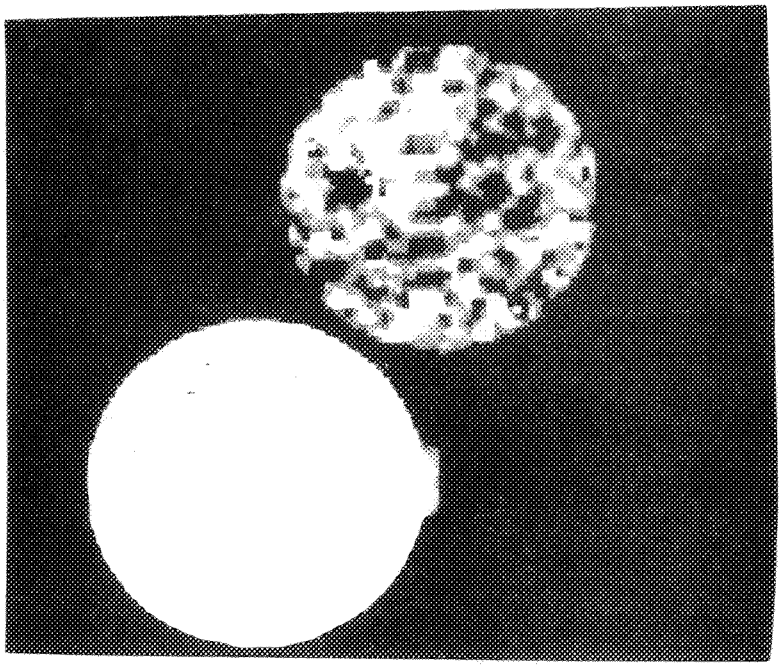

Figure 7. Separated (a) water and (b) oil images of the three Bentheim sandstone cores with 100% water saturation (lower right), 100% oil saturation (lower left) and mixed water/oil saturation (top).

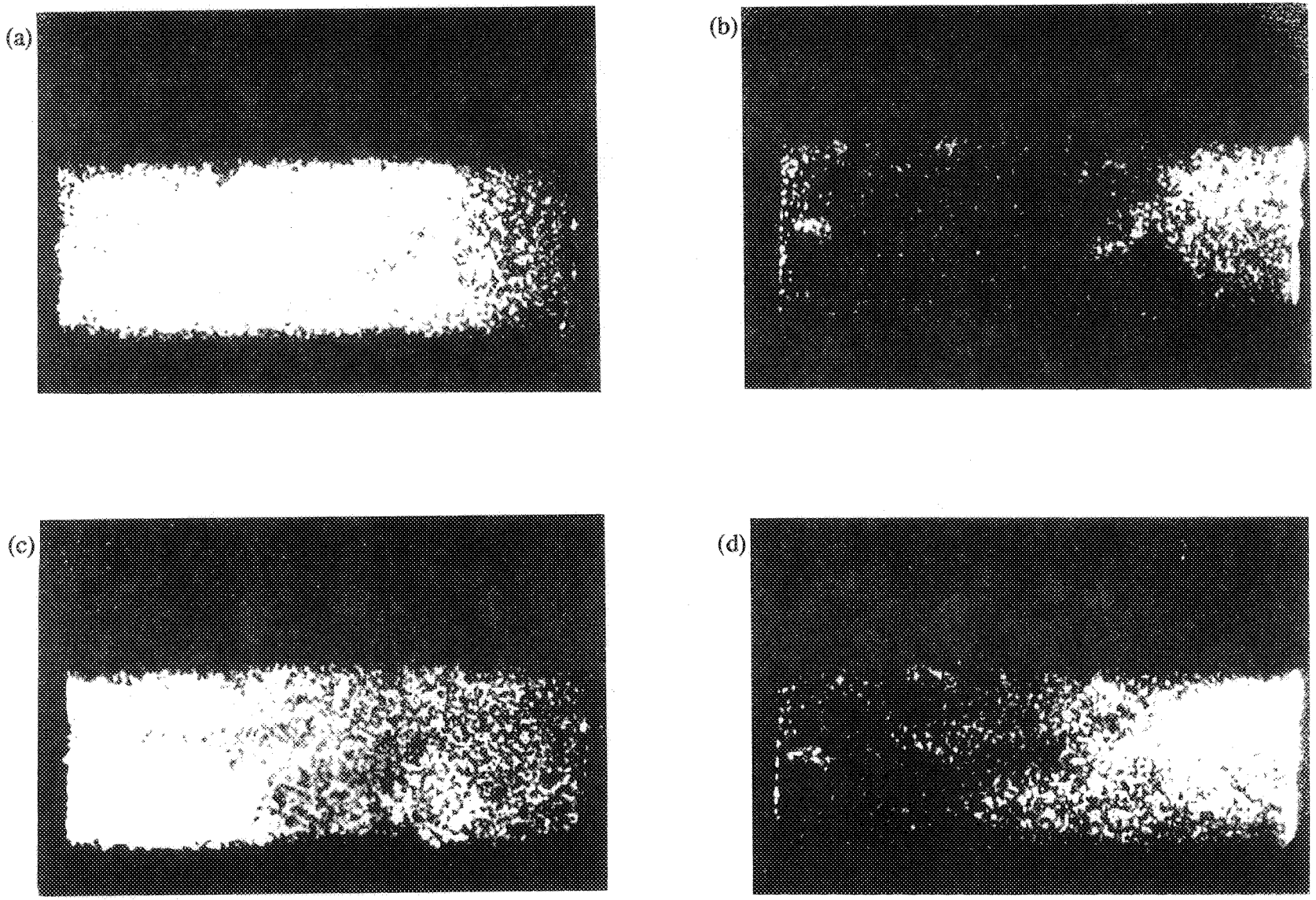

Figure 8. (to be continued)

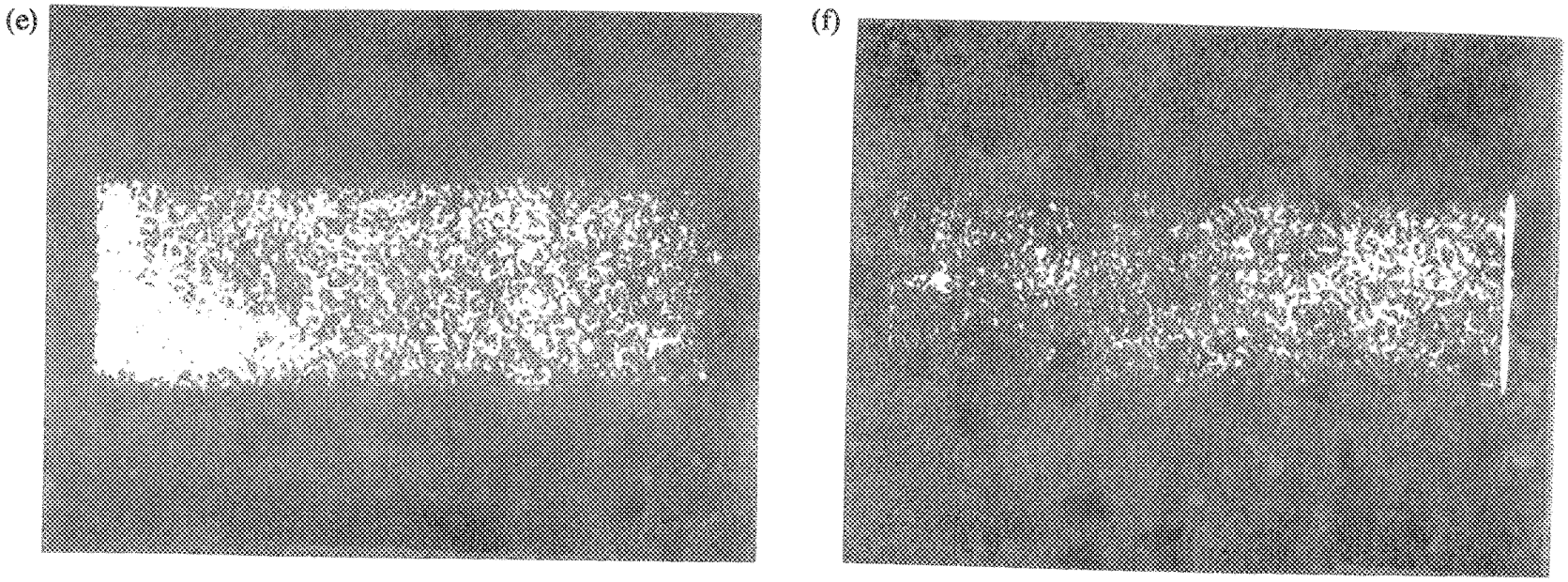

Figure 8. Separated water and oil images of the carbonate sample at successive stages of the oil-flooding experiment. (a), (c), and (e) are water images; (b), (d) and (f) are oil images. Artifacts at the left of the core in the oil images are caused by the phase wraparound problem.

1991 SCA Conference Paper Number 9114

PROTON MR TWO - COMPONENT CHEMICAL SHIFT IMAGING OF FLUIDS IN POROUS MEDIA

C.T. Chang and C.M. Edwards
Engineering Imaging Laboratory
Texas A&M University
College Station, TX 77843-3116

ABSTRACT

An NMR chemical shift imaging modality is presented for quantitative determination of the spatial distribution of water and oil saturation in porous samples. It is applicable to those samples for which the two resonance lines overlap severely, and for which significant signal decay occurs during the chemical shift evolution period. We have used this method to demonstrate the separation of water and oil images in sand packs and core samples.

INTRODUCTION

Magnetic resonance imaging (MRI) has the potential to provide a means to determine the spatial distribution of fluid saturations within opaque porous media, with obvious applications in rock physics, fluid/rock interfacial processes, and porous media fluid dynamics, especially liquid - liquid displacement mechanics. In order to study the multiphase flow, where several fluid phases may be present within the pore space, it is necessary to distinguish between fluids of different chemical compositions.

During the last few years, several approaches for achieving this result have been investigated. Hall et al.[1] performed a study in which they obtained resolved images of water and oil in a sandstone based on the difference in relaxation times. However, it is necessary that the protons in different phases have different relaxation times. Relaxation times of fluids in porous media are dominated by fluid/surface interactions and pore geometry[2], resulting in a wide distribution of relaxation times as well as a decrease in the difference of relaxation times between water and oil. Consequently, the available contrast for fluid identification based on relaxation times is considerably reduced. A number of other workers have reported NMR images of water and oil distributions in porous samples utilizing the chemical shift interaction. The various methods for chemical shift imaging can be classified into two major categories. The first category consists of methods that selectively excite or saturate water (or oil) protons before a conventional imaging pulse sequence is applied. Edelstein, et al.[3] have demonstrated the use of selective excitation to observe oil and water in saturated dolomite cores. The selective saturation method has been used by Dechter, et al.[4] to obtain specific images for Bakers dolomite and Bentheim sandstone core. The spectrally selective pulses again yield images of only one fluid phase at a time. The second category involves methods of spectroscopic chemical - shift imaging, in which a chemical - shift dimension is added to each voxel. Conventional chemical - shift imaging uses two spatial orthogonal phase - encoding magnetic field gradients and collects free induction decay signals in the absence of magnetic field gradients.[5] Hall et al.[6] used this technique to observe dodecane and water in Berea sandstone samples. The full three - dimensional chemical - shift imaging methods are rarely used because of long experiment times, unless relatively coarse spatial resolution is acceptable. If high spectral resolution is not desired, the data acquisition efficiency can be enhanced significantly by frequency encoding one of the space dimensions and phase encoding the chemical shift. In a spin - echo sequence this is usually done by changing the amplitude of the magnetic field gradient pulse[7] or by varying the time of the 180° pulse while keeping the time between excitation and acquisition constant.[8] By making one of these changes a

time delay is inserted between the Hahn spin - echo and gradient echo allowing the magnetization vectors to evolve out of phase with each other by an amount dependent on the spectral frequency differences. If this period is incremented in regular steps, the spectral frequency will be encoded as a phase change, yielding the desired spectrum upon Fourier transformation. Majors, et al.[9] reported the use of the echo - time - encoded spectroscopic imaging technique to study the displacement of oil by water - flooding in a dolomite core sample.

It can be seen that the application of all the above techniques is limited to those samples for which the NMR line broadening is moderate and spectral resolution is still observable. Horsfield, et al.[10] presented an estimation method based on the phase shift technique to observe water and dodecane in a Hopeman sandstone. This method provides the ability to distinguish two chemically - shifted components even when the spectral lines cannot be resolved. Well - characterized spectra and a large amount of computing power are required to be successful using this technique. In addition the quantification of the intensity of the NMR signal is problematical. We present here an improvement upon Horsfield's technique for chemical shift imaging which provides the capability to rapidly and easily quantify the oil and water NMR signals in porous media where their resonance lines are not baseline separated.

THEORY AND METHODS

The imaging sequence used was a modified spin - warp spin - echo sequence (Fig. 1) into which a variable chemical - shift evolution time τ is introduced. The gradient echo always occurs at a time t when

$$\int_0^t G(\tau')\, d\tau' = 0. \qquad (1)$$

It is at this time that the frequency encoded position information is in phase. All other frequency encoded information such as chemical shift and inhomogeneous line broadening are in phase at the Hahn spin echo time. Deliberately allowing the Hahn echo and the gradient echo to occur at different times is the method for introducing the chemical - shift evolution time τ. Using the knowledge of the chemical shift between oil and water, a phase shift of the respective signals can be achieved by suitable adjustment of Hahn spin - echo time relative to gradient echo time . Since a chemical - shift dimension is generated only to resolve the different fluids, high spectral resolution is not required. As demonstrated by Dixon,[11] two steps of evolution period may be adequate to resolve two fluid phases.

The Dixon method, however, suffers from two drawbacks with respect to quantitative accuracy when applied to fluids in porous media. First, when chemical - shift evolution takes place, factors other than chemical shift can cause additional phase shifts. These factors include inhomogeneity of the static magnetic field, magnetic susceptibility variations and nonuniform phase delays caused by instrumentation factors such as induced eddy currents of time dependent magnetic fields. Second, during the period of chemical shift evolution the signal from each pixel will decay with time constant T_2^*, where T_2^* is associated with the linewidth for the pixel in question. Therefore, to quantitatively resolve water and oil signals it is necessary to (a) remove the contribution of phase errors due to nonchemical shift mechanisms, and (b) take into consideration the signal decay.

Let (x,y) be coordinates in the laboratory frame of reference, which is perpendicular to the slice selection direction z. In the two dimensional spin warp Fourier transform MRI technique, the free induction decay signal can be expressed as[8]

$$S(t,G_y) = \int d\omega \int dx \int dy\ \rho(x,y,\omega)$$
$$\exp\{i[(\omega + \Delta)(t+\tau) + \gamma G_x x t + \gamma G_y y t_y + \alpha]\}\ , \tag{2}$$

where G_x and G_y are the gradients in x and y directions, respectively; γ is the gyromagnetic ratio; $\Delta(x,y)$ is the frequency offset due to the magnetic field inhomogeneity; t_y is the time for which the phase encoding gradient G_y is switched on; and $\alpha(x,y)$ is the nonuniform phase delays caused by instrumentation factors. The expression $\rho(x,y,\omega)$ is the spin density including the relaxation effects, where ω is written explicitly to specify that the image signal is subject to the linewidth and chemical shift effects. The signal is collected as a function of time t after the read gradient G_x is on. One may show[12] that Eq. 2 is the result of neglecting the fact that the protons with different chemical shift are excited at slightly different positions along the z-axis corresponding to their resonance frequencies. Therefore, Eq. 2 may be used within experimental error when a sufficiently large z-gradient is applied during the excitation period. This condition for the slice definition is assumed throughout this paper.

An NMR image is obtained by Fourier transforming Eq. 2 with respect to G_y and t. One can see that the conjugate variable of G_y is $\gamma y t_y$, which is readily transformed to y since γ and t_y are known quantities. However, the Fourier transform variable of t is $(\omega + \Delta + \gamma G_x x)$; thus the effects of linewidth, chemical shift and field inhomogeneity are to spread out the signal in the x-direction in the image. For a sufficiently strong gradient G_x, the misregistration in the readout direction can be small. In this work this offset is less than 1 pixel. Under this condition the image intensity for each pixel is of the form

$$S(x,y) = \left\{\int \rho(x,y,\omega)\, e^{i\omega\tau}\, d\omega\right\} \cdot \exp\{i(\Delta \cdot \tau + \alpha)\}\ . \tag{3}$$

When a sample consists of two chemical components with chemical shift δ_k and lineshape function $f_k(\omega)$, $\rho(x,y,\omega)$ can be partitioned into two parts, $\sum_{k=1,2} \rho_k(x,y)\, f_k(\omega - \delta_k)$, and Eq. 3 can be rewritten as follows:

$$S(x,y) = \left\{\sum_{k=1,2}\left[\int f_k(\omega')\, e^{i\omega'\tau}\, d\omega'\right] \rho_k(x,y)\, e^{i\delta_k\tau}\right\} \cdot \exp\{i(\Delta \cdot \tau + \alpha)\}\ , \tag{4}$$

where $\omega' = \omega - \delta_k$. The integration

$$g_k(\tau) = \int f_k(\omega') e^{i\omega'\tau} d\omega' \quad , \tag{5}$$

which is the Fourier transform of the lineshape function, represents a decay factor of the signal during the period τ. For a Lorentzian lineshape, the decay factor is simply exp $(-|\tau| / T_2^*)$.

If the transmitter reference frequency is placed at the nominal precessional frequency of water protons, Eq. 4 becomes

$$S(x,y) = \{g_w(\tau)\rho_w + e^{i\delta\tau} g_o(\tau) \rho_o\} \cdot \exp\{i(\Delta \cdot \tau + \alpha)\} , \tag{6}$$

where $g_{w,o}$ and $\rho_{w,o}$ are the signal decay factor and spin density, respectively, for water/oil; and δ is the chemical shift of oil signal relative to water signal. The transmitter is not required to be at the water proton frequency. If some offset exist it is simply added to Δ.

The in - phase ($\delta\tau = 0$) and opposed - phase ($\delta\tau = \pi$) images can be used to determine the position dependent phase factor $\Delta \cdot \tau$. To do this, the phase errors α caused by instrumentation factors are first removed from the opposed - phase image by rotating the intensity vector of each pixel by an angle $-\alpha$, where α is the phase angle of the corresponding pixel in the in - phase image. A phase slope method[13] is then used to remove any abrupt 180° transitions in the phase of the opposed - phase image at water/oil interfaces. This leaves only the smooth phase shifts $\Delta \cdot \tau$. Phase unwrapping is required in the cases when $\Delta \cdot \tau$ is of such magnitude that phase wraparound problem must be confronted, which often occur for images of large cross - sectional area or for samples with large magnetic susceptibilities.

Instead of using in - and opposed - phase images to obtain segregated water and oil images, two more images are acquired by shifting the Hahn spin - echo before and after the field gradient echo, giving symmetric 90° phase shift of the oil magnetization vector with respect to the water vector. By so doing, the problem of different signal decay factors can be minimized since the chemical - shift evolution time is the same in both image data sets. The images are phase corrected with phase map $\Delta \cdot \tau$ /2, where $\Delta \cdot \tau$ is obtained from the opposed-phase image. In accordance with Eq. 6, vector diagrams of the magnetic moments with $\delta\tau = \pm$ 90° in the rotating frame are drawn, as shown in Fig. 2. The phase shifts due to field inhomogeneities have been corrected and the phase delay α is not shown for clarity. At each voxel the signal, S(x,y), will have decayed because of the T2* effects. This is represented by spreading of vectors representing oil and water magnetization. In the figure these line widths of the oil and water resonances are equal. Because the net magnetization for the oil/water components is the vector sum of the oil/water isochromats, net magnetization will be ±90° out of phase regardless of the oil/water linewidths

There are two points to be noted in Fig. 2. First, in general cases the water and oil resonance lines can be overlapping. Second, the signal decay factor is determined by the lineshape and can be different for the two fluids. When the lineshapes for the two fluids are different, then quantification is difficult unless the linewidths have been determined independently. For fluids in porous media the linewidth is dominated by microscopic field gradients caused by the static susceptibility difference between the fluids and the rock matrix combined with the random geometry of the pore space.[14] If the aqueous phase does not have too many dissolved

paramagnetic impurities then the static susceptibility of the aqueous phase and the oil phase should not be very different and the linewidths of the two phases would therefore be approximately equal. But even under the conditions where the linewidths are significantly different, it is apparent from the diagrams that the vector sum and difference of these two image data sets yield the completely separated component vectors. The final separated images can then be formed in magnitude to eliminate the phase factor α.

RESULTS AND DISCUSSION

All measurements were performed on a General Electric 2T CSI system operating at 85.56 MHz, with an Oxford instrument superconducting magnet of 31 cm diameter horizontal bore, supported by a Nicolet 1280 computer together with a Nicolet 293F pulse programmer. Magnetic field gradients were provided by a shielded Accustar gradients set with 200 μs settling time. An 11 cm birdcage RF probe was used for both radiofrequency transmission and reception of the NMR signal.

The pulse sequence used is shown in figure 1. It is an ordinary 2-D spin warp sequence except the Hahn - echo time is allowed to vary while the gradient - echo time is kept fixed. This is accomplished by changing the timing of the 180° inversion pulse. Precise control over the oil/water phase shift is possible using this method. The only limitation is that t must be much less than T2 in order to neglect T2 effects in the analysis of the data.

The first porous sample used in this study was a composite sample which was made from a cylindrical vial (1.0 cm i.d. and 3.5 cm length) of Ottawa sand (50 - 70 mesh). Water and machine oil were absorbed separately into the two halves of the sample. By examining the NMR spectrum, it was observed that the proton resonances of water and oil are separated by 3.5 ppm and the linewidth at half-maximum for each of the resonances was estimated to be approximately 2.4 ppm. The longitudinal relaxation times T_1 for the water and oil in the sample were measured to be 133 and 116 ms, respectively. The transverse relaxation times T_2 were measured using the Hahn sequence and were found to be 20 and 28 ms, respectively. One - dimensional projection images were taken along the cylindrical axis of the sample which is in the vertical direction. The time between the 90° pulse and the center of the gradient echo is 4 ms. In order to achieve a 180° phase shift between the oil and water resonances, an evolution time of 1.6 ms was used. Two hundred fifty -six complex points were collected during the echo, giving a resolution of 0.17 mm. Figure 3 is an in phase image upon magnitude calculation. The water occupies the lower part of the sample and the interface between water and oil is in the vicinity of the 120th pixel. Figure 4 compares the present method with the Dixon method. Fig. 4 (a) and (b) were calculated by summing and subtracting the in - phase and opposed - phase image vectors, respectively. It is noted that some oil intensities remain in the water image and likewise, some water intensities are seen in the oil image. As mentioned earlier, the artifact is due to static field inhomogeneity errors as well as the difference in the signal decay factors between in - and opposed - phase images. Fig. 5 is a phase map of inhomogeneity and magnetic susceptibility as calculated from the opposed - phase image. It is a function which varies smoothly over the sample with discontinuities at the boundary between the sample and the surrounding area. The effect of the magnetic field inhomogeneity on the pore - size scale can be averaged over each pixel because the pixel size is generally larger than the pore size. Fig. 4 (c) and (d) are the true water and oil images, respectively, obtained using our method, which show a clear separation of the two fluids.

Next, we demonstrated the ability of this method to resolve two chemically distinct fluids coexisting as immiscible phases intimately mixed in the same pore space. The rock samples used in this experiment were Bentheim sandstone, the cores being 2.54 cm in diameter and 4.7 cm long and having a porosity of 23%. Three identical cores were prepared: the first one was 100% saturated with 5% sodium chloride solution (specific gravity 1.034); the second one was 100%

saturated with Soltrol 130 (specific gravity 0.754); whereas the third one was flushed through with approximately 31 pore-volumes of Soltrol 130 after the 100% brine saturation. Fig. 6 shows a spectrum from the third sample. The linewidth for each resonance was measured from the single - fluid saturated samples to be 3.2 ppm for water and 3.3 ppm for oil, satisfying the requirement for quantification of the fluid phase. The relaxation times T_1 and T_2 are 628 ms (716 ms) and 16.6 ms (19.1 ms) for the water (oil) saturation, respectively. Transverse slice images with three samples bundled together were taken. The slice - select gradient was 1.94 G/cm, which gave a slice thickness of 5 mm. One hundred twenty - eight complex points were sampled in the presence of 3 G/cm readout gradient, which, combined with 128 increments of the phase - encoding gradient gave an in - plane resolution of 0.5 mm. The time between the excitation pulse and acquisition was 3.6 ms. A phase map associated with the magnetic field inhomogeneity was calculated from the phase difference between the opposed - and in - phase image data sets, and which was subsequently used in the correction of the ± 90° phase - shifted image data. Fig. 7 shows the separated water and oil images obtained by using our method. The water and oil signal intensities were then calculated from the NMR images by summation of the pixel intensities over the regions of the images in which the cores sit. The results are shown in Table 1, together with the values calculated from the ordinary image. The remaining intensity of the 100% water (oil) saturated sample in the oil (water) image is less than 4%. If we treat the cores which contain single - fluid saturation as standard references, the combined signal intensity from water and oil in the mixed saturated core is found to be in excellent agreement with the value obtained from the ordinary image.

Table 1. Average Signal Intensity in Bentheim Sandstone

Sample	Chemical - Shift Image		Ordinary Image
	Water Image	Oil Image	
Background	599	586	423
Water saturated	25,538	1,005 (3.9%)	15,239
Oil saturated	1,063 (3.8%)	28,247	17,792
Water & Oil Saturated	13,722	11,728	15,606

We have also used this method to study the oil - flooding of the water saturated rock sample. A cylindrical sample of carbonate (2.5 cm diameter, 5.5 cm length) was oven dried at 70°C for 24 hours and then vacuum saturated with 2% sodium chloride solution. At this stage, the water saturation was 100% and the porosity of the sample was found to be approximately 20%. The core was then inserted into a plastic core holder with a Hassler sleeve and an external pressure of 120 psi was applied on the Hassler sleeve and so maintained during the entire experiment. The core was injected with machine oil at a rate of 0.1 ml/min using an HPLC pump. The NMR spectrum linewidth is 236 Hz at 2 Tesla, and T_1 and T_2 are respectively 123 and 7.6 ms. Two hundred fifty - six phase - encoding steps and 256 complex points were sampled in the presence of a 5G/cm gradient in the flow direction (Z - direction), which allowed the time between 90° pulse and acquisition to be reduced to 4.3 ms and gave an in - plane resolution of 0.27 mm. Again the slice thickness was 5 mm. With eight averages for each image data the experiment time was 17 minutes. The flow was interrupted during the performance of the experiments. Fig. 8 shows a time - lapse series of the spatially resolved water and oil saturations of the water displacement by oil in the core. The horizontal direction is Z which corresponds with the readout gradient, the cylindrical axis of the core, the direction of the applied magnetic field, and the direction of the flow (from right to left), whereas the vertical direction is Y. The displacement of water by oil is seen to proceed with well - behaved phase boundaries. The field inhomogeneity correction algorithm was successfully applied to each image data, though the opposed - phase image has reduced amplitude

in those regions where the water and oil coexist, resulting in a relatively noisy phase map. In case the signal intensity for the opposed - phase image is too weak to produce a useful phase map, a phase correction can be performed using the one generated from the data set where the water saturation was 100%. [10]

CONCLUSION

An efficient method of chemical shift imaging has been presented. The method involves only a simple modification of the technique described by Horsfield together with a phase correction algorithm. It can easily be extended to a multislice experiment by using slice-selective excitation pulses in the usual way. One of the main advantages of this method is its availability of quantitatively mapping water and oil distribution in porous rocks even when the resonance lines overlap. Another advantage is time efficiency as compared to a full three-dimensional chemical shift imaging experiment. One disadvantage is that an opposed phase image with poor signal-to-noise ratio may result from regions where the signal intensities from the water and oil are approximately the same, making the phase correction difficult. We have successfully demonstrated the quantitative separation of water and oil images in sand packs and some rock samples. The chemical shift imaging technique described here appears to improve the possibility of quantitative analysis of the spatial distribution of the fluid phases in core samples.

REFERENCES

1. L.D. Hall and V. Rajanayagam, Thin - Slice, Chemical - Shift Imaging of Oil and Water in Sandstone Rock at 80 MHz, Journal of Magnetic Resonance **74**, 139 (1987)

2. F. D'Oraxio, J.C. Tarczon, W.P.Halparin, K. Eguchi, and T. Mizusaki, Application of Nuclear Magnetic Resonance Pore Structure Analysis to Porous Silica Glass, J. Appl. Phys. **65**, 743 (1989)

3. W.A. Edelstein, H.J. Vinegar, P.N. Tutunjan, P.B. Roemer and O.M. Mueller, NMR Imaging for Core Analysis: SPE 18272, 63rd Annual Technical Conference and Exhibition, October 1988

4. J.J. Dechter, R.A. Komoroski and S. Ramaprasad, NMR Chemical Shift Selective Imaging of Individual Fluids in Sandstone and Dolomite Cores, SCA Conference paper number 8903, 1989

5. L.D. Hall and S. Sukumar, Three - dimensional Fourier Transform NMR Imaging, J. Magn. Reson., **56**, 314 (1984)

6. L.D. Hall, V. Rajanayagan, and C. Hall, Chemical - Shift Imaging of Water and n-Dodecane in Sedimentary Rocks, J. Magn. Reson., **68**, 185 (1986)

7. J.J. Ford, Gradient - Amplitude Phase - Encoded Spectral Imaging. A Novel Approach to Spin - Echo Chemical - Shift Imaging, J. Magn. Reson., **87**, 346 (1990)

8. C.C. Lodes, J.P. Felmlee, R.L. Ehman, C.M. Sehgal, J.F. Greenleaf, G.H. Glover, and J.E. Gray, Proton MR Chemical Shift Imaging Using Double and Triple Phase Contrast Acquisition Methods, Journal of Computer Assisted Tomography **13(5)**, 855 (1989)

9. P.D. Majors, J.L. Smith, F.S. Kovarik, and E. Fukushima, NMR Spectroscopic Imaging of Oil Displacement in Dolomite, J. Magn. Reson, **89**, 470 (1990)

10. M. Horsfield, C. Hall, and L.D. Hall, Two - Species Chemical - Shift Imaging Using Prior Knowledge and Estimation Theory. Application to Rock Cores, J. Magn. Reson., **87**, 319 (1990)

11. W.T. Dixon, Simple Proton Spectroscopic Imaging, Radiology **153**, 189 (1984)

12. A. Volk, B. Tiffon, J. Mispelter, and J. M. Lhoste, Chemical Shift Specific Slice Selection, A New Method for Chemical Shift Imaging at High Magnetic Field, J. Magn. Reson., **71**, 168 (1987)

13. J.A. Borrello, T.L. Chenevert, C.R. Mayer, A.M. Aisen, and G.M. Glazer, Chemical Shift - based True Water and Fat Images: Regional Phase Correction of Modified Spin - Echo MR Images, Radiology, **164**,531 (1987)

14. J.A. Glael and K.H. Lee, On the interpretation of water nuclear magnetic resonance relaxation times in heterogeneous systems, J. Am. Chem. Soci., **96(4),** 970 (1974)

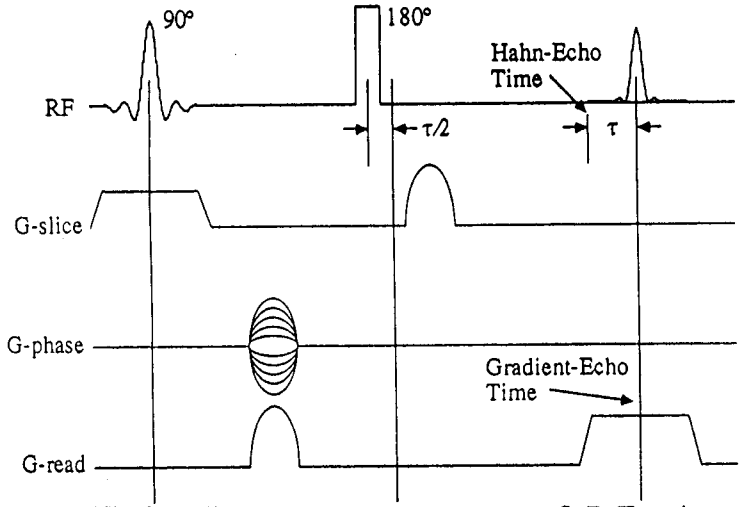

Figure 1. Timing diagram for phase-encoded 2-D Fourier transform chemical-shift imaging pulse sequence.

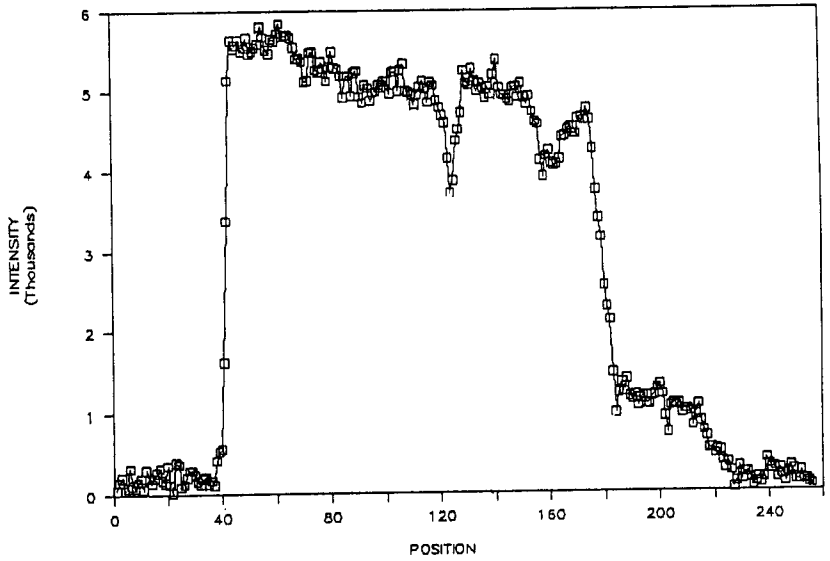

Figure 3. Conventional 1-D profile image of the composite sand pack sample. The magnitude calculation was carried out to obtain the image of water and oil.

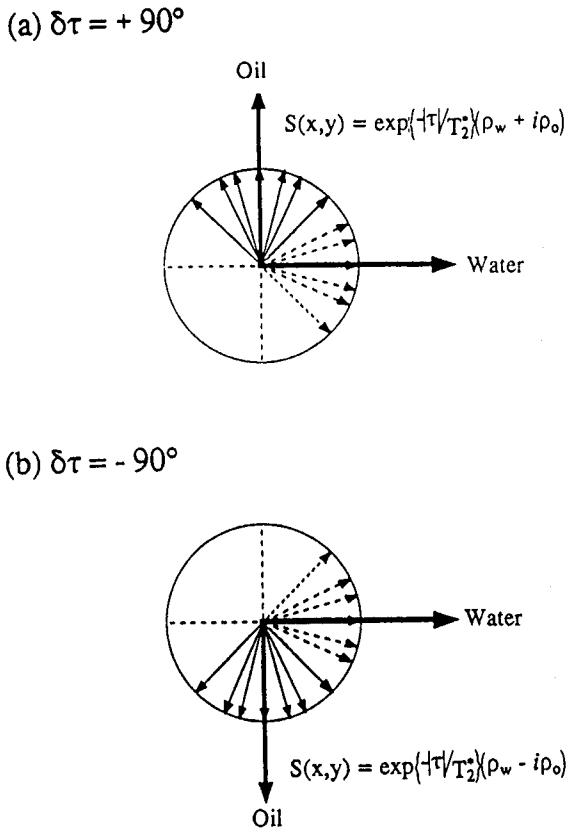

Figure 2. Proton magnetic moments for a pixel containing both water and oil, representing the signals obtained at times when (a) $\delta\tau = +90°$ and (b) $\delta\tau = -90°$. They are drawn in a frame rotating at the water proton frequency. The dashed vectors represent water magnetization and the solid vectors represent oil magnetization.

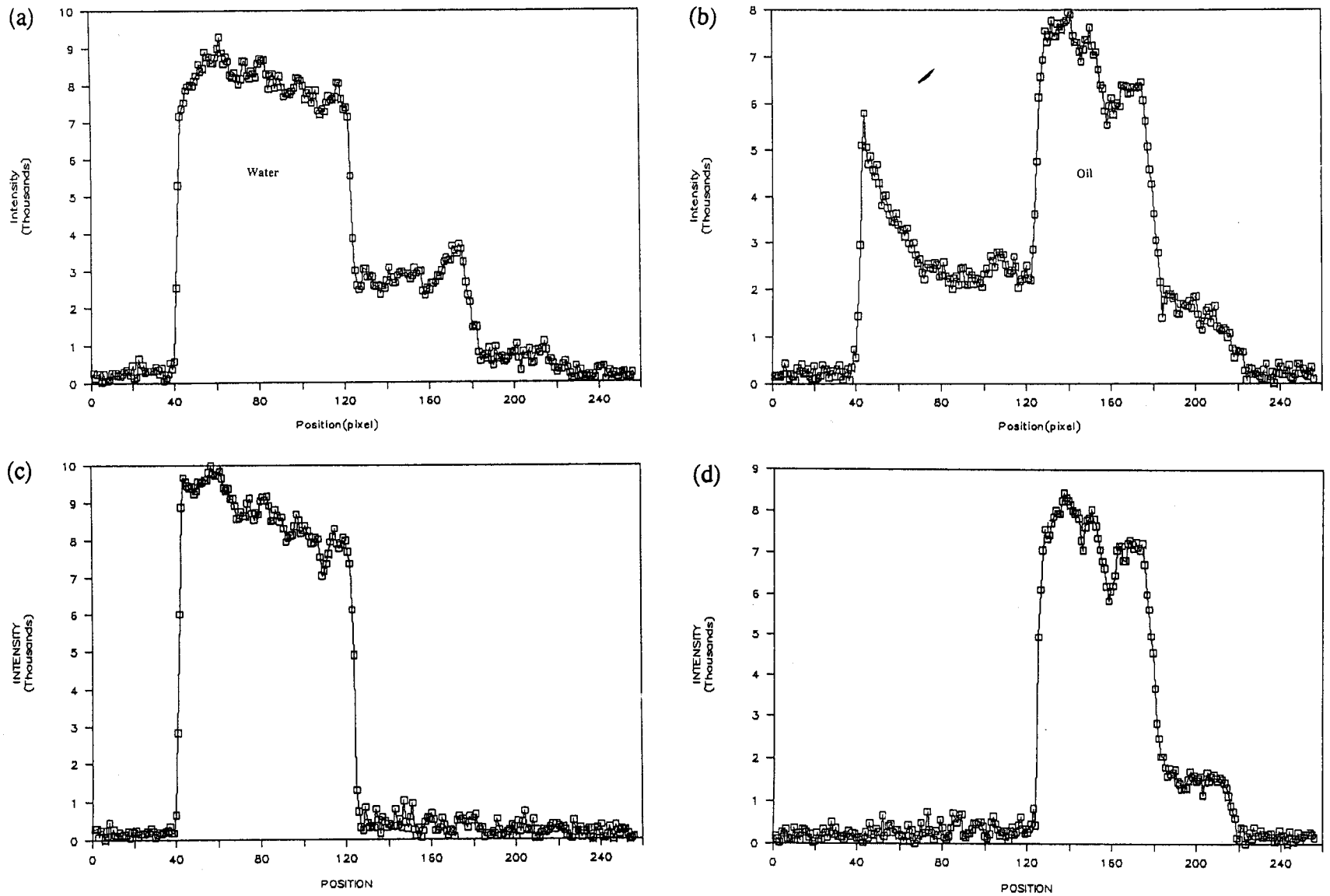

Figure 4. Chemical-shift 1-D profile images of the sand pack sample containing water and machine oil. (a) and (b) are the water and oil images, respectively, obtained using magnitude-of-sum and difference techniques (Dixon's technique). (c) water image, and (d) oil images obtained using method described in the text.

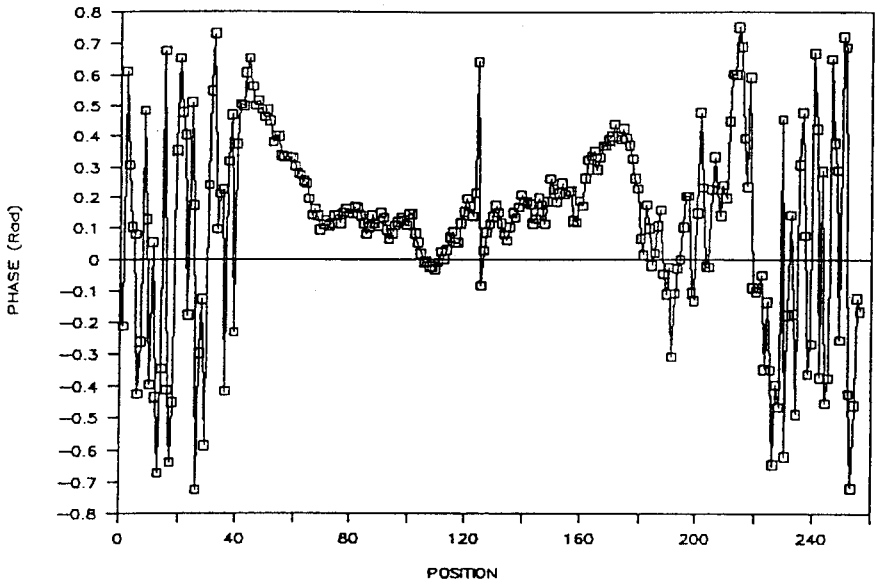

Figure 5. One-dimensional phase map of the sand pack sample showing the nonchemical-shift phase effects.

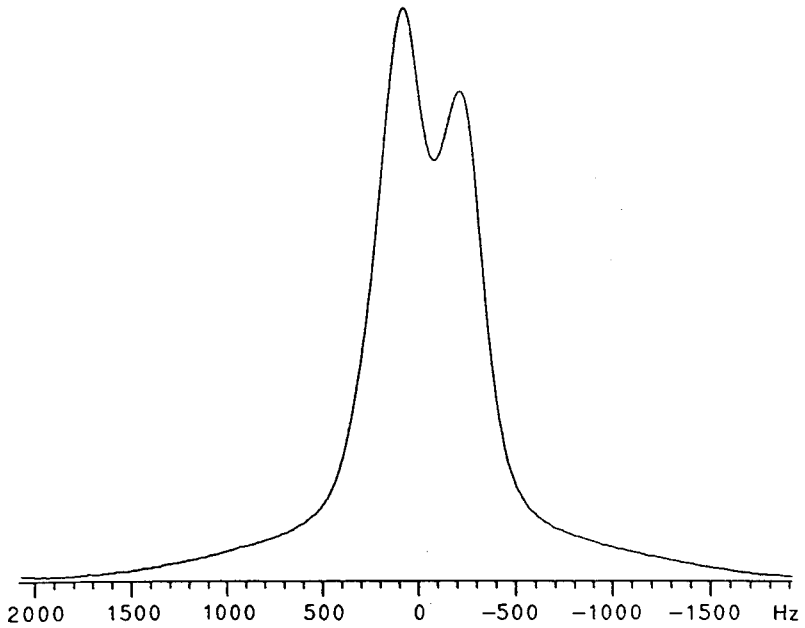

Figure 6. NMR spectrum taken from the whole Bentheim sandstone sample with mixed oil and NaCl solution saturations.

(a)

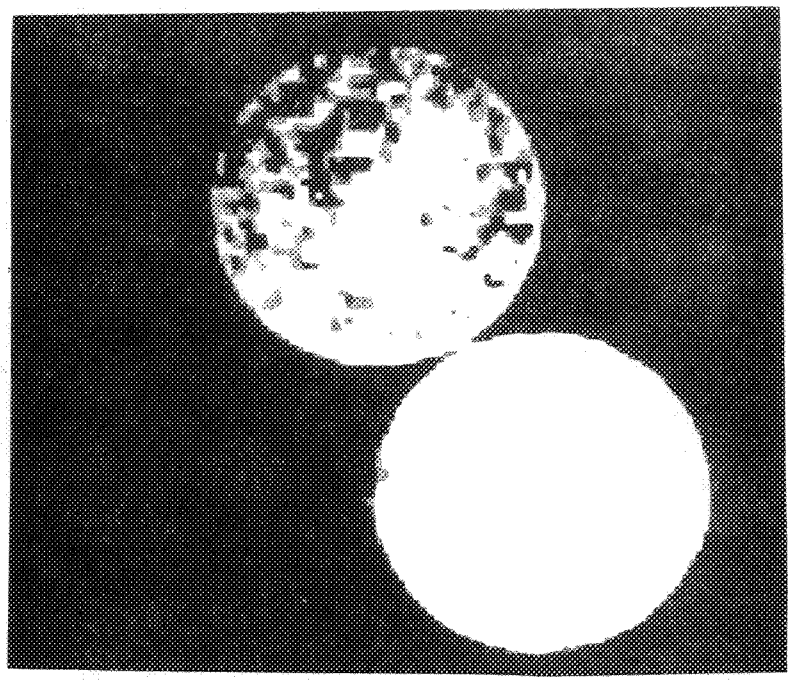

(b)

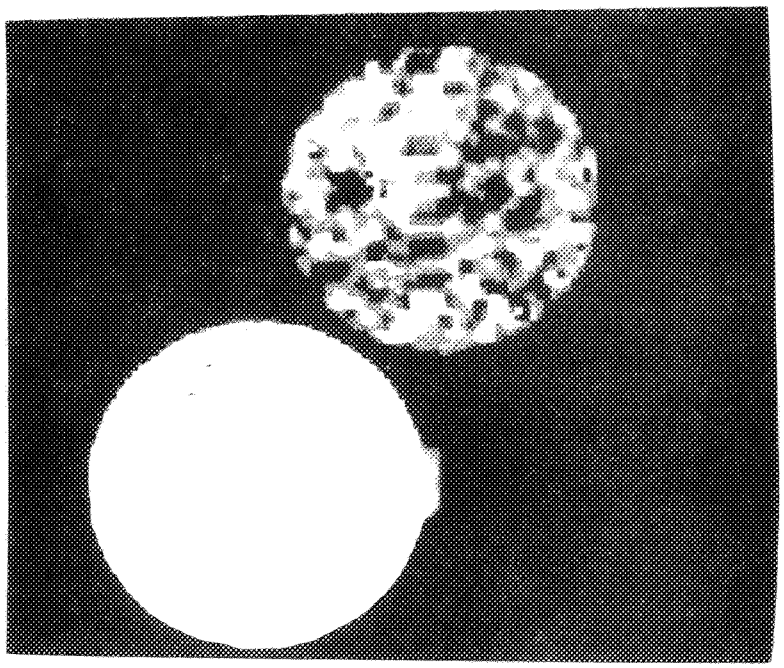

Figure 7. Separated (a) water and (b) oil images of the three Bentheim sandstone cores with 100% water saturation (lower right), 100% oil saturation (lower left) and mixed water/oil saturation (top).

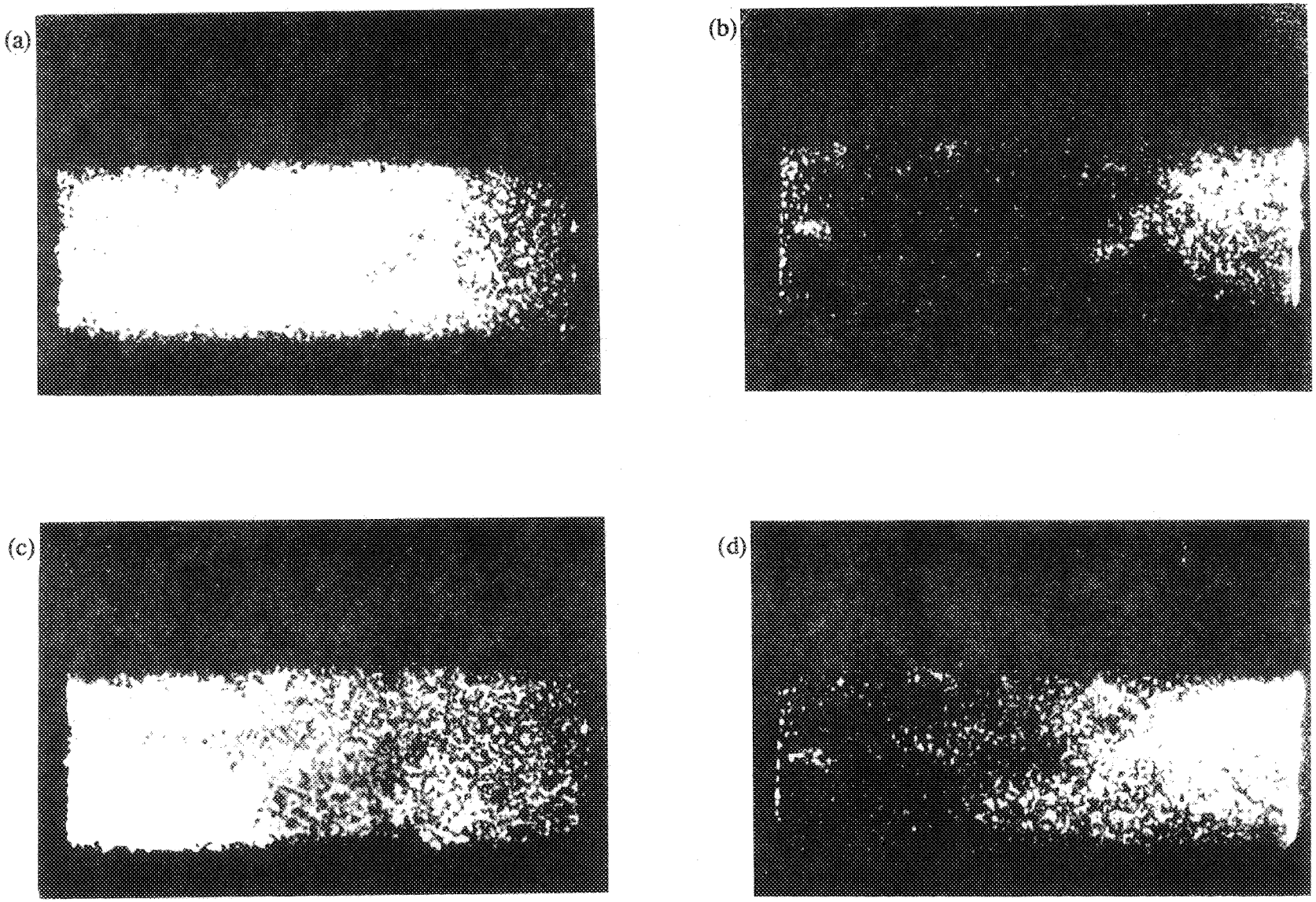

Figure 8. (to be continued)

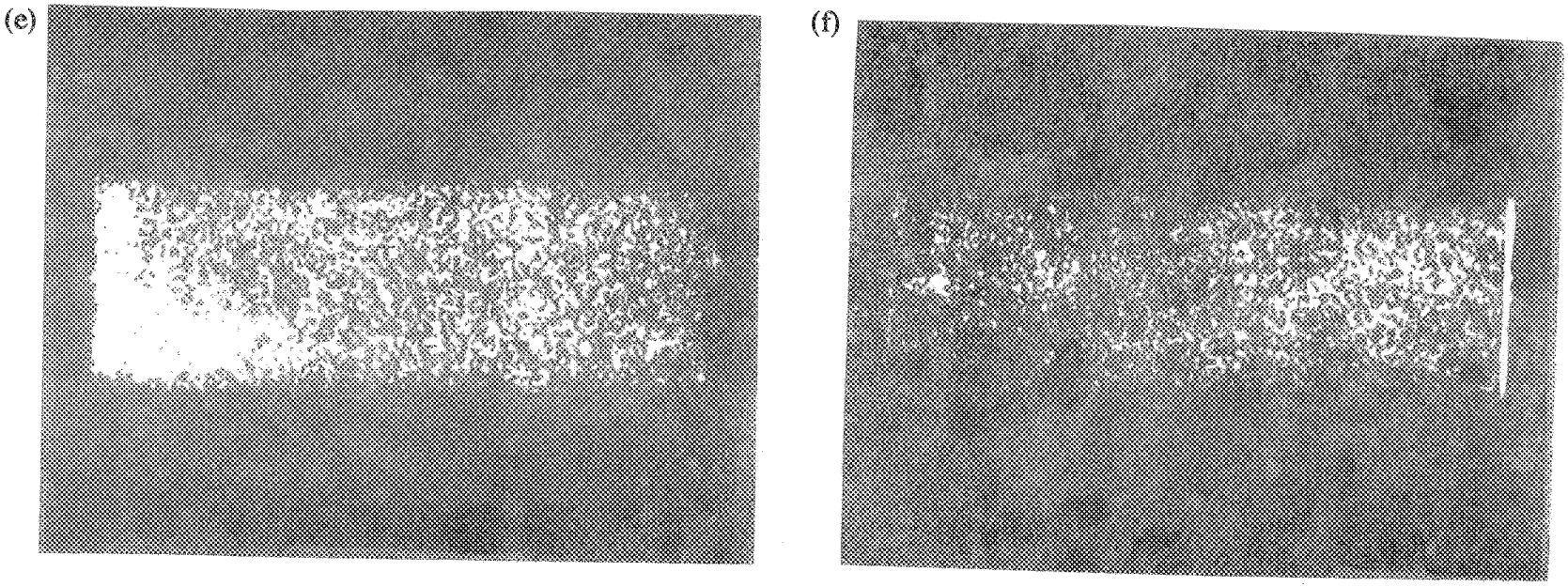

Figure 8. Separated water and oil images of the carbonate sample at successive stages of the oil-flooding experiment. (a), (c), and (e) are water images; (b), (d) and (f) are oil images. Artifacts at the left of the core in the oil images are caused by the phase wraparound problem.